Hindawi
Shock and Vibration
Volume 2018, Article ID 9202153, 11 pages
https://doi.org/10.1155/2018/9202153

Research Article

The Unbalanced Radial Force of In-Wheel Switched Reluctance Motors Effect on Vehicle Performance under Stability Condition

Yanyang Wang, Funing Yang, Fuxing Shang, and Qing Xiong

The Key Laboratory of Automotive Engineering, Xihua University, Chengdu 610039, China

Correspondence should be addressed to Yanyang Wang; yywang@mail.xhu.edu.cn and Qing Xiong; xiong_qiming@163.com

Received 3 January 2018; Revised 4 July 2018; Accepted 29 August 2018; Published 1 November 2018

Academic Editor: Jussi Sopanen

This paper studies the unbalanced radial force of in-wheel switched reluctance motors effect on vehicle performance under stability condition. First, the IWM-EV vehicle model which highlights the new factors of the rotor, stator, SRM vertical force, and airgap deflection was adopted. And the vehicle comparison models were established to make a contrastive study about IWM-EV new structure effects. Then, Routh's stability criterion method was adopted to judge the vehicle system's stability condition. It includes two parts: characteristic polynomial of the vehicle system which is served to calculate the IWM-EV system Routh array and Routh's stability criterion which is used to judge the vehicle system's stability condition. The effect of the new structure on vehicle performance was further discussed under stability condition. It mainly includes two aspects: vehicle vibration mode analysis which is used to study vehicle vibration characteristics and amplitude-frequency analysis which is served to research transfer response characteristics of the vehicle system. The result shows that the new structure of IWM-EV has a negative effect on vehicle stability performance. The SRM vertical force will change vehicle stability characteristic. In some severe cases, it will even destroy IWM-EV's stability.

1. Introduction

Nowadays, the in-wheel motor electric vehicle (IWM-EV) has attracted more and more interest as a powerful solution to energy and environmental problems. Many research studies focus on taking full advantage of IWM-EV. For example, vehicle stability control [1, 2], vibration and comfort issue [3, 4], moment control, and power consumption [5, 6]. However, there are also some issues that need to be further studied. It mainly includes unsprung mass-increasing problem, torque ripple, and motor vibration issues.

As the key component of the propulsion system, the electric motor plays an important role in IWM-EV dynamics. Permanent magnet (PM) motors are popular, being used in electric vehicles as driven motor due to its excellent advantages: compact size, high-power density, and efficiency. However, compared with the switched reluctance motor (SRM), PM motors' costs are significantly higher. Its performance is more sensitive to temperature. Besides that, SRM does not require PMs which contribute to the simple and rugged construction [7]. Nowadays, SRM gets more and more attention as the in-wheel motor due to its excellent advantages: a simple structure, ruggedness, fault tolerance ability, high-speed operation capability, high-power density, and low manufacturing cost. However, these advantages are overshadowed by its inherent torque ripple, vibration, and noise, which seriously hindered the applications of SRM for in-wheel motor [8–11].

SRM has two different structures: radial SRM and axial SRM. Generally speaking, radial and axial SRMs have the same operating concepts, except the orientation of the flux as it passes through the rotor. The flux is parallel to the axis of rotation in axial motors and perpendicular in radial machines. For radial SRMs, the unbalanced radial force will affect vehicle vertical dynamics, which will directly influence vehicle comfort performance and tyre dynamic load. The tyre dynamic load will further affect vehicle stability. However, for the axial SRMs, the unbalanced radial force will affect vehicle lateral and longitudinal dynamics, which directly affects vehicle rollover stability and drive

performance. In this paper, we mainly focus on the unbalanced radial force of radial SRMs effect on vehicle dynamics. The residual unbalanced radial force caused by airgap eccentricity, namely SRM vertical force, is one of the main reasons for radial SRM vibration [12–14].

To suppress SRM vibration, some structures and controllers are investigated. Jian Li and Cho [13] proposed a method to reduce the unbalanced radial force and vibration of SRM by introducing parallel paths in windings. These results revealed that the currents can be balanced in parallel paths and unbalanced radial force could be reduced. Inagaki et al. [14] proposed a two-degree-of-freedom H∞ control to suppress vehicle drive train vibration. Furqani et al. [15] focus on the effect of saturation on SRM radial force and vibration. These existing research studies contribute to suppress SRM vibration; however, the SRM vibration effect on vehicle stability and comfort is seldom considered. The role and effect of stability and comfort such as the unbalanced radial force of SRM in rollover analysis need to be considered further. This paper focuses on SRM vibration effect on vehicle performance. For the convenience of analysis, we consider the severe case of unbalanced radial force. So the windings in parallel, the controller, the saturation issue, and other structure problems are not taken into consideration in this paper.

SRM vertical force and airgap deformation are the two main reasons in wheel motor vibration. In the previous work [16–18], the effect of SRM vertical force and control methodology has been investigated, but the new structure of electric vehicles effect on vehicle system stability needs to be further discussed. Following the previous work, this study will consider the IWM-EV system stability performance, with the organization as follows: the IWM-EV vehicle model which highlights the new factors of the rotor, stator, SRM vertical force, and airgap deflection was adopted. And the vehicle comparison models were established to make a contrastive study about IWM-EV new structure effects. Then, Routh's stability criterion method was adopted to judge the stability condition of the vehicle system. The effect of the new structure on vehicle performance was discussed under stability condition.

2. Vehicle Modeling

The primary objective of this study is to understand the new structure effects mentioned above; the required IWM-EV dynamics model thus needs to reflect the contributions of those new factors. In this study, the vehicle modeling consists of two parts: (i) the IWM-EV vehicle model that highlights the new factors of the rotor, stator, SRM vertical force, and airgap deflection and (ii) the vehicle comparison models that neglect the new factor of SRM vertical force, the rotor, or stator on vehicle vibration, which are used to make a contrastive study about IWM-EV new structure effects.

2.1. Quarter Vehicle Model. To simulate the rotor, stator, SRM vertical force, and airgap deformation effect on IWM-EV dynamic responses, the quarter vehicle model is developed as shown in Figure 1. The reference vehicle is a four wheel-driven sedan. The sprung mass is fixed on the strut, denoted by m_1.The mass of the wheel is divided into two parts: one is SRM stator and housing mass, named "static mass" and denoted by m_2; the other is the total mass of tyre, hub, and SRM rotor, named "rotating mass" and denoted by m_3. The two parts are connected by the hub bearing. In order to simplify the model, the two bearings are reduced to one where stiffness k_2 is the sum of SRM and hub bearing. The damping is ignored because it is relatively small. The vertical component of SRM unbalanced force F_v was named 'SRM vertical force'. It is exerted between static mass m_2 and rotating mass m_3. It will affect SRM airgap deformation, thereby further affecting SRM and vehicle performance. The details can be seen from the previous work [16–18].

The governing equations of the vehicle body vibration and roll motions can be described as

$$m_1\ddot{z}_1 = -c_1(\dot{z}_1 - \dot{z}_2) - k_1(z_1 - z_2), \quad (1)$$

$$m_2\ddot{z}_2 = c_1(\dot{z}_1 - \dot{z}_2) + k_1(z_1 - z_2) - k_2(z_2 - z_3) - F_v, \quad (2)$$

$$m_3\ddot{z}_3 = k_2(z_2 - z_3) - c_3(\dot{z}_3 - \dot{q}) + k_3(z_3 - q) + F_v. \quad (3)$$

In the equations above, the coordinates defined in the model are corresponding to their loaded positions. z_1, z_2, and z_3 denotes m_1, m_2, and m_3, vertical displacement from its static equilibrium state, respectively; q is the effective road profile displacement input at the tyre-road interface. The vehicle parameter values used for this study are listed in Table 1.

2.2. IWM-EV Model

2.2.1. SRM Vertical Force Model. The well-known 6/4 outside-rotor SRM [19, 20] is used in this study. The vertical force generated by SRM eccentricity is shown in Figure 2 [3]. Its mechanism and characteristics can be found in the previous work [3, 16, 18]. To shorten, only the important equations are given in this paper.

The unbalanced radial force is due to the difference between a pair of opposite stator poles. According to [21], the radial force of opposite stator poles can be described as follows:

$$F_1 = -\frac{\sin(\theta_o)}{g_m - \Delta g}T, \quad (4)$$

$$F_2 = -\frac{\sin(\theta_o)}{g_m + \Delta g}T. \quad (5)$$

The unbalanced radial force is

$$F_r = F_1 - F_2. \quad (6)$$

The vertical component of the unbalanced radial force is SRM vertical force, F_v, which is

$$F_v = F_r \sin(\theta'), \quad (7)$$

where T is wheel-driving torque, which is determined by vehicle-driving conditions, g_m is the airgap length of SRM,

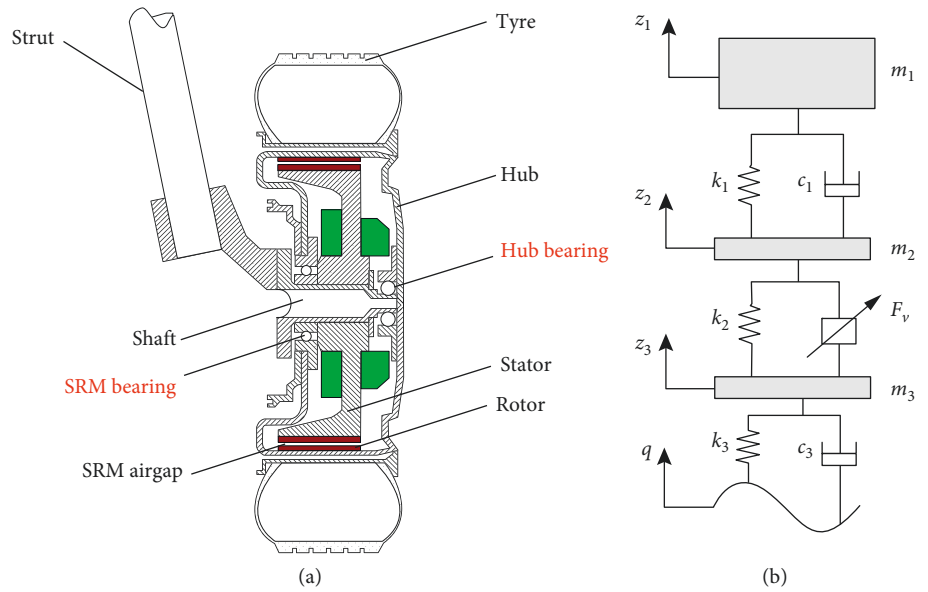

Figure 1: The quarter vehicle model. (a) In-wheel motor structure. (b) In-wheel mass spring-damper model.

Table 1: Vehicle nomenclature and value.

Definition	Symbol	Units	Value
Sprung mass	m_1	kg	340
SRM stator	m_{21}	kg	10
SRM housing mass	m_{22}	kg	30
SRM rotor mass	m_{31}	kg	10
Tyre and hub mass	m_{32}	kg	40
Stiffness suspension	k_1	N/m	27358
Stiffness of SRM and hub bearing	k_2	N/m	8×10^6
Stiffness tyre	k_3	N/m	309511
Damping suspension	c_1	N·s/m	1695
Damping of tyre	c_3	N·s/m	100
Effective radius of wheel	R	m	0.269
SRM airgap	g_m	m	0.008

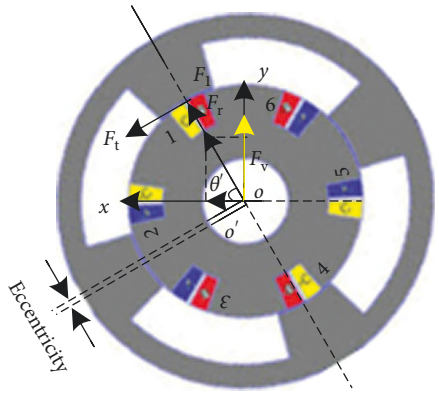

Figure 2: SRM vertical force.

and θ' is the angle between F_r and wheel longitudinal axis. In the actual working condition, the unbalanced radial force is distributed along the stator radius. And each pair of opposite rotors with eccentricity can generate unbalanced radial force. So the θ' is variable. If θ' is a positive value, it means the direction of radial force F_r is located in the upward half plane x-y, whose range is $[0, \pi]$. Conversely, if θ' is a negative value, it means the direction of F_r is located in the upward half plane x-y, whose range is $[-\pi, 0]$. θ_o is the stator and rotor pole overlap position. Δg is the airgap eccentricity, also called as the airgap deformation. It is equal to the relative displacement of the M_{msij} and M_{uij}:

$$\Delta g = z_2 - z_3. \tag{8}$$

According to Equations (4)–(7), SRM vertical force F_v can be rewritten as

$$F_v = T\sin(\theta')\sin(\theta_o)\left(\frac{1}{g_m - \Delta g} - \frac{1}{g_m + \Delta g}\right). \tag{9}$$

2.2.2. SRM Vertical Force Linearization. Due to introduction of the nonlinear term $((1/g_m - \Delta g) - (1/g_m + \Delta g))$, the IWM-EV model changes from linear differential equations into nonlinear differential equations. The nonlinear differential equations analysis such as Runge–Kutta method [22] or polynomial method [23] is more suitable for a thorough investigation. However, for simplicity, here the nonlinear term is approximated as a linear term using Taylor expansion methods.

In real-driven condition, the airgap relative eccentricity $((\Delta g/g_m)\times 100\%)$ maximum is 30%~60% [24, 25], which means airgap deformation is less than 0.48 mm for the reference SRM ($0.8\,\text{mm}\times 0.6 = 0.48\,\text{mm}$). Otherwise, the SRM is destructed due to the rotor impact. In other words, the absolute value of $\Delta g/g_m$ is less than 0.6 ($|\Delta g/g_m| \le 0.6$). According to Taylor expansion approximation method [26],

$$\frac{1}{1-x} = 1 + x + x^2 + \frac{x^3}{1-x} \quad |x| \le 1. \tag{10}$$

The nonlinear term $((1/g_m - \Delta g) - (1/g_m + \Delta g))$can be approximated as the following equation:

$$\begin{aligned} \text{Nonterm} &= \left(\frac{1}{g_m - \Delta g} - \frac{1}{g_m + \Delta g}\right) \\ &= \frac{1}{g_m}\left(\frac{1}{1 - \Delta g/g_m} - \frac{1}{1 + \Delta g/g_m}\right) \approx \frac{2\Delta g}{g_m^2}. \end{aligned} \tag{11}$$

And the approximation error is

$$\text{Error} = \frac{2x^3}{1 - x}. \tag{12}$$

Figure 3 shows the comparison of the nonlinear term between true value and approximate value and the error. It can be seen that the approximate value is near to the true value, especially in the small value of airgap deformation. So, it is reasonable to substitute the approximate value to the true value.

Substituting Equations (8) and (11) into Equation (9), SRM vertical force $F_v$can be approximated as the following equation:

$$F_v = k_v(z_2 - z_3). \tag{13}$$

The coefficient k_v is familiar with spring stiffness, named equivalent coefficient of SRM vertical force, which is as follows:

$$k_v = T\sin(\theta')\sin(\theta_0)\frac{2}{g_m^2}. \tag{14}$$

According to Equation (13), the form of SRM vertical force is familiar with spring force. The equivalent coefficient k_v varies according to the wheel-driving torque T, the angle θ', and the overlap position θ_o. To a four wheel-driven sedan, the range of each wheel-driving torque T is about [0, 400 Nm] [27]. To 6/4 SRM, the range of θ_o is $[0, \pi/6]$. The range of θ' is $[-\pi, \pi]$. So, the maximum and minimum value of equivalent coefficient k_v is about 6.25×10^8 N/m and -6.25×10^8 N/m $(400\,\text{Nm} \times \sin(\pm\pi/2) \times \sin(\pi/6) \times 2/g_m^2 = \pm 6.25 \times 10^8\,\text{N/m})$, respectively.

Ultimately, the IWM-EV movement equations (1)–(3), (13), and (14) are linear differential equations, the analysis methods of linear differential equations can be adopted conveniently.

2.3. Vehicle Comparison Models. To make a contrastive study about the effect of SRM stator, rotor, airgap deformation, and vertical force on vehicle dynamics, two models are considered: (i) the Model A considering SRM stator and rotor as a rigid unit part, neglecting SRM vertical force and SRM airgap deformation, which is similar with the conventional centrally driven vehicle dynamics model; (ii) the Model B taking SRM stator and rotor as two parts, considering SRM airgap deformation and SRM vertical force.

In Model A, the motor stator and rotor is considered as a unit part and the motor rigid fixed on the wheel. Vehicle unsprung mass m_2' is the sum of m_2 and m_3 $(m_2' = m_2 + m_3)$. And the vertical movement of m_2' is denoted by z_2'. Equation (2) is rewritten as

$$m_2'\ddot{z}_2' = c_1(\dot{z}_1 - \dot{z}_2) + k_1(z_1 - z_2) + c_3(\dot{z}_3 - \dot{q}) + k_3(z_3 - q). \tag{15}$$

The differences between these three models are shown in Table 2.

3. The New Structure Effect on IWM-EV System Stability

In order to analyze the new structure effect on IWM-EV system stability, the Routh's stability criterion method was adopted here due to its simple and efficient characteristics [28]. It mainly includes two aspects: characteristic polynomial of the vehicle system which is served to calculate IWM-EV system Routh array; Routh's stability criterion which is used to judge stability condition of the vehicle system.

3.1. Vehicle System Characteristic Polynomial. The state-space equations of Model A and Model B can be derived from vehicle movement differential equations. Taking Model B as an example, the vehicle vibration equations (1)–(3), (13), and (14) can be written as a state-space form:

$$\dot{X} = AX + BU, \tag{16}$$

where

$$A = \begin{bmatrix} 0 & 1 & 0 & 0 & 0 & 0 \\ -k_1/m_1 & -c_1/m_1 & k_1/m_1 & c_1/m_1 & 0 & 0 \\ 0 & 0 & 0 & 1 & 0 & 0 \\ k_1/m_2 & c_1/m_2 & -(k_1 + k_2 + k_v)/m_2 & -c_1/m_2 & (k_2 + k_v)/m_2 & 0 \\ 0 & 0 & 0 & 0 & 0 & 1 \\ 0 & 0 & (k_2 + k_v)/m_3 & 0 & -(k_2 + k_v + k_3)/m_3 & 0 \end{bmatrix},$$
$$X = \begin{bmatrix} z_1 & \dot{z}_1 & z_2 & \dot{z}_2 & z_3 & \dot{z}_3 \end{bmatrix}^T,$$
$$B = \begin{bmatrix} 0 & 0 & 0 & 0 & 0 & k_3/m_3 \end{bmatrix}^T. \tag{17}$$

It is important to note that the equivalent coefficient k_v is variable, and the variation range is $[-6.25 \times 10^8\,\text{N/m}, 6.25 \times 10^8\,\text{N/m}]$ as discussed in Section 2.2.2. And the other vehicle parameters are determined which are listed in Table 1. So, the characteristic polynomial of state-space matrix A is a mathematical expression of the equivalent coefficient

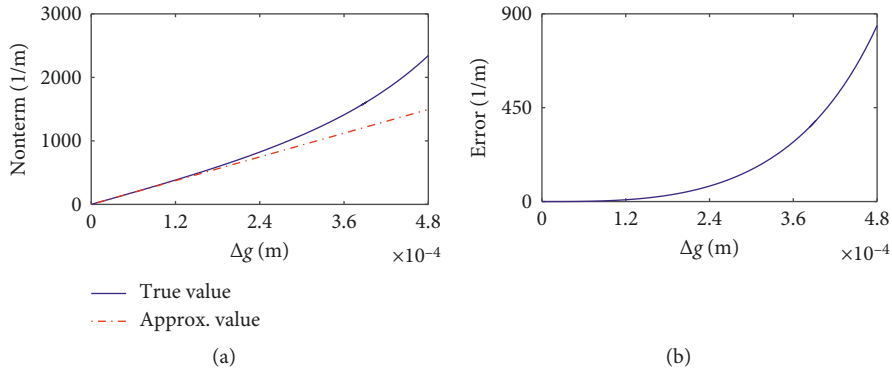

Figure 3: Comparison of nonlinear term between true value and approximate value. (a) Comparison between true value and approximate value. (b) Error between true value and approximate value.

Table 2: The differences between three vehicle models.

Model type	Description	Equations
Model A	Neglecting SRM vertical force Neglecting SRM airgap deformation	Equations (1) and (15)
Model B	Considering SRM vertical force Considering SRM airgap deformation	Equations (1)–(3), (13), and (14)

k_v. Equating the characteristic polynomial to zero, the characteristic equation of matrix A can be obtained

$$a_0 s^6 + a_1 s^5 + a_2 s^4 + a_3 s^3 + a_4 s^2 + a_5 s^1 + a_6 = 0, \quad (18)$$

where $a_0 = 1$, $a_1 = 29.49$, $a_2 = 0.045k_v + 3.67 \times 10^5$, $a_3 = 0.6722k_v + 5.56 \times 10^6$, $a_4 = 172.2k_v + 1.38 \times 10^9$, $a_5 = 451.9k_v + 3.62 \times 10^9$, $a_6 = 12452k_v + 9.96 \times 10^{10}$.

According to the same method, the characteristic equation of Model A can be calculated. Since the coefficient k_v is not taken into consideration in Model A, the characteristic equation of Model A is a constant coefficient equation. It is different with that of Model B.

3.2. Routh's Stability Criterion. Routh's stability criterion is a powerful and simple method to judge system stability characteristics [28]. According to Routh's stability criterion, a necessary and sufficient condition for Equation (16) to be a stability system is all the coefficients in the first column of the Routh array should be positive. The Routh array is derived from the characteristic polynomial equation (18). It can be described as

$$\begin{matrix} a_0 & a_2 & a_4 & a_6 \\ a_1 & a_3 & a_5 & a_7 \\ b_1 & b_2 & b_3 & 0 \\ c_1 & c_2 & 0 & 0 \\ d_1 & d_2 & 0 & 0 \\ e_1 & 0 & 0 & 0 \\ f_1 & 0 & 0 & 0 \end{matrix}, \quad (19)$$

where $b_1 = a_1a_2 - a_0a_3/a_1$, $b_2 = a_1a_4 - a_0a_5/a_1$, $b_3 = a_1a_6 - a_0a_7/a_1$, $c_1 = b_1a_3 - a_1b_2/b_1$, $c_2 = b_1a_5 - a_1b_3/b_1$, $d_1 = c_1b_2 - b_1c_2/c_1$, $d_2 = c_1b_3/c_1$,$e_1 = d_1c_2 - c_1d_2/d_1$,$f_1 = e_1d_2/e_1$.

So the stability condition of the vehicle system in Equation (16) is

$$\begin{cases} a_0 > 0, \\ a_1 > 0, \\ b_1 > 0, \\ c_1 > 0, \\ d_1 > 0, \\ e_1 > 0, \\ f_1 > 0. \end{cases} \quad (20)$$

It is a set of inequalities including the equivalent coefficient k_v. Solving inequalities in Equation (20), the stability condition of the vehicle system can be calculated, which is an inequality related to the equivalent coefficient k_v. The sign of the first column coefficients of the Routh array of Model B is summarized in Table 3. It is worth to note that the critical point of vehicle stability is $k_v = -8 \times 10^6$ N/m. It is equal and opposite to SRM and hub-bearing stiffness value $k_2 = 8 \times 10^6$ N/m. In this case, the static mass m_2 is suspended. In the critical point case, the vehicle system changes from stability system to unstability system. It is necessary to point out that the critical system is a special kind of unstability system.

In order to further study the new structure effect on vehicle stability performance, three typical cases, e.g., stability system, unstability system, and critical stability system, were picked up and are listed in Table 4. The equivalent coefficients k_v are set to -8.2×10^6 N/m in Case 1, which is an unstability system according to Table 3. Similarly, in order to get critical stability system and stability system, equivalent coefficients k_v are set to -8×10^6 N/m and -8.2×10^6 N/m, respectively.

The coefficients in the first column of the Routh array of Case 1, Case 2, and Case 3 of Model B and Model A can be calculated by Equations (16), (18), (19), which are summarized in Table 5.

Table 3: The sign of the first column coefficients of Routh array.

The sign of the first column coefficients	Stability characteristics
$k_v \in (-8 \times 10^{-6}$ N/m, 6.25×10^{-8}] N/m keep positive	Stability
$k_v = -8 \times 10^{-6}$ N/m have zero	Critical stability
$k_v \in [-6.25 \times 10^{-8}$ N/m, -8×10^{-6}) N/m have negative	Unstability

Table 4: Three typical vehicle systems.

Model type	The equivalent coefficients (k_v)	Stability characteristics
Model B (Case 1)	$k_v = -8.2 \times 10^{-6}$ N/m	Unstability system
Model B (Case 2)	$k_v = -8 \times 10^{-6}$ N/m	Critical stability system
Model B (Case 3)	$k_v = -7.8 \times 10^{-6}$ N/m	Stability system

Tables 3 and 5 show that the first column coefficients of the Routh array of Model A are always positive. However, the vehicle stability is determined by the equivalent coefficient k_v in Model B. If the equivalent coefficient k_v belongs to the range of (-8×10^6 N/m, 6.25×10^8 N/m), all the coefficients of the first column of the Routh array are positive. The vehicle is the stability system. Otherwise, the nonpositive value appears. And the stability of the vehicle system is lost. This means that the equivalent coefficient k_v will change vehicle stability characteristics. In other words, SRM vertical force will affect vehicle stability performance. It will even destroy IWM-EV stability in some severe cases. Without stability, vehicle safety, comfort, maneuverability, and other performance are not possible.

4. The New Structure Effect on Vehicle Performance under Stability Condition

As mentioned above, SRM vertical force will destroy vehicle system stability. To guarantee vehicle system stability, SRM vertical force must be fully considered in vehicle practical control and design process. So the effect of the new structure on vehicle performance needs to be further discussed under stability condition. It mainly includes two aspects: vehicle vibration mode analysis which is used to study vehicle vibration characteristics; and amplitude-frequency analysis which is served to research vehicle system transfer response characteristics.

4.1. Vibration Mode Analysis. For comparative analysis of vehicle vibration mode, the vehicle models Model A and Model B need to be transformed into the undamped vibration form. Taking Model B as an example, the vehicle vibration equations (1)–(3), (13), and (14) can be written as a undamped free vibration form:

$$M\ddot{Z} + KZ = 0. \tag{21}$$

Here,

$$M = \begin{bmatrix} m_1 & 0 & 0 \\ 0 & m_2 & 0 \\ 0 & 0 & m_3 \end{bmatrix},$$

$$K = \begin{bmatrix} k_1 & -k_1 & 0 \\ -k_1 & (k_1 + k_2 + k_v) & -k_2 \\ 0 & -k_2 & (k_2 + k_3 + k_v) \end{bmatrix}, \tag{22}$$

$$Z = \begin{bmatrix} z_1 \\ z_2 \\ z_3 \end{bmatrix}.$$

The characteristic equation of the vehicle system is

$$\left| M^{-1}K - \omega^2 I \right| = 0, \tag{23}$$

where ω^2 are the eigenvalues and ω are the angular natural frequencies of IWM-EV vibration. The eigenvectors are the shapes of these vibrational modes.

Based on Equation (23), the natural frequency of Model B is calculated, which is shown in Figure 4. It can be seen that the third-order natural frequency of Model B increases with equivalent coefficient. There is a power function relationship between SRM vertical force equivalent coefficient k_v and the third-mode natural frequency ω_3. This means that the third natural frequency was introduced by the SRM vertical force and airgap deformation. It will cause a new resonance region, which will further affect vehicle vibration. And SRM vertical force and airgap deformation will be affected reversely. The resonance frequency increased with the equivalent coefficient k_v of SRM vertical force. It is worth to point out that if the equivalent coefficient k_v is near to the critical point ($k_v = -8.0 \times 10^6$), the third natural frequency is near to the first and second natural frequencies, which is easy to cause the vertical resonance of vehicle body, rotating mass, and static mass. On the other hand, if the equivalent coefficient k_v is large, the third natural frequency is large which will affect tyre-rotating vibration [29].

The vibration energy distributions of Model A and Model B (Case 3) ($k_v = -8.2 \times 10^6$) are calculated via Equation (23), as shown in Tables 6 and 7. It can be seen that the first and second natural frequencies basically remain constant, about 1.28 Hz and 8.63 Hz, respectively. They are broadly consistent with that of Model B, which are 1.37 Hz and 9.76 Hz, respectively. And the third natural frequency is 18.11 Hz. Accordingly, the vibration energy focuses on wheel static mass and rotating mass, 27.52% and 72.45%, respectively. It means that the rotating mass will resonate at 18.11 Hz in Model B (Case 3).

The vibration modes of Model A and Model B (Case 3) are also calculated via Equation (23), as shown in Figures 5 and 6, respectively. Figure 5 shows that the sprung mass vibration prevails at the first-mode shape. And the unsprung mass vibration prevails at the second-mode shape. Comparing with Figure 6, the sprung mass vibration takes predominance at the first-mode shape. And the static and

Table 5: The first column coefficients of Routh array.

	a_0	a_1	b_1	c_1	d_1	e_1	f_1
Model A	1	13.83	3.10×10^3	8.72×10^3	2.77×10^5	—	—
Model B (Case 1)	1	29.49	-3.25×10^3	-2.04×10^5	-2.48×10^7	-9.25×10^7	-2.49×10^9
Model B (Case 2)	1	29.49	1.19×10^3	5.42×10^4	4.37×10^6	9.46×10^6	0
Model B (Case 3)	1	29.49	5.63×10^3	1.17×10^5	3.24×10^7	6.83×10^7	2.49×10^9

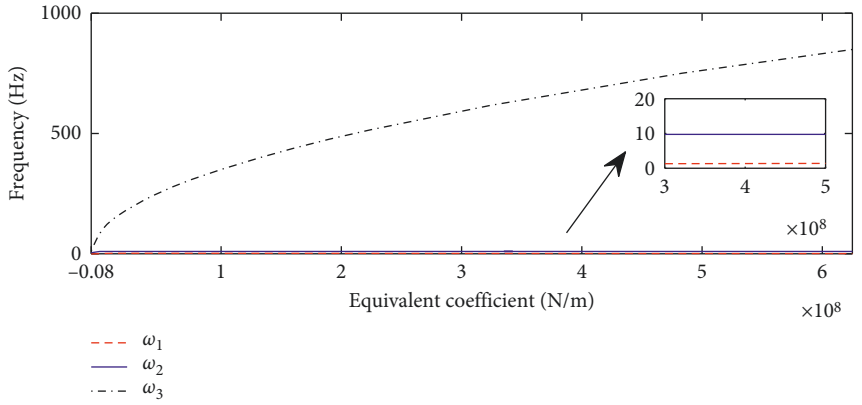

Figure 4: The natural frequency of Model B.

Table 6: Vibration energy distribution of Model A.

	Natural frequency (Hz)	Sprung mass vibration energy (%)	Unsprung mass vibration energy (%)
1st mode	1.3672	99.8186	0.1814
2nd mode	9.7458	0.1814	99.8186

Table 7: Vibration energy distribution of Model B (Case 3).

	Natural frequency (Hz)	Sprung mass vibration energy (%)	Static mass vibration energy (%)	Rotating mass vibration energy (%)
1st mode	1.28	99.5069	0.4126	0.0805
2nd mode	8.63	0.4839	72.0698	27.4463
3rd mode	18.11	0.0091	27.5176	72.4732

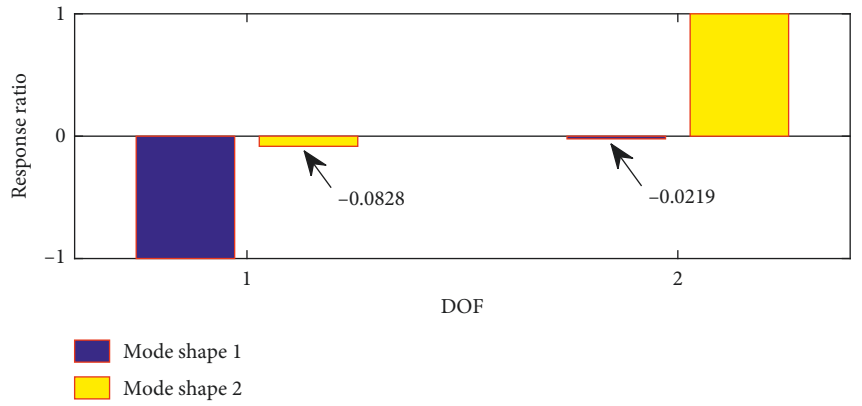

Figure 5: Vibration modes of Model A. Mode 1: 1.37 Hz; mode 2: 9.75 Hz; dof1: sprung mass; dof2: unsprung mass.

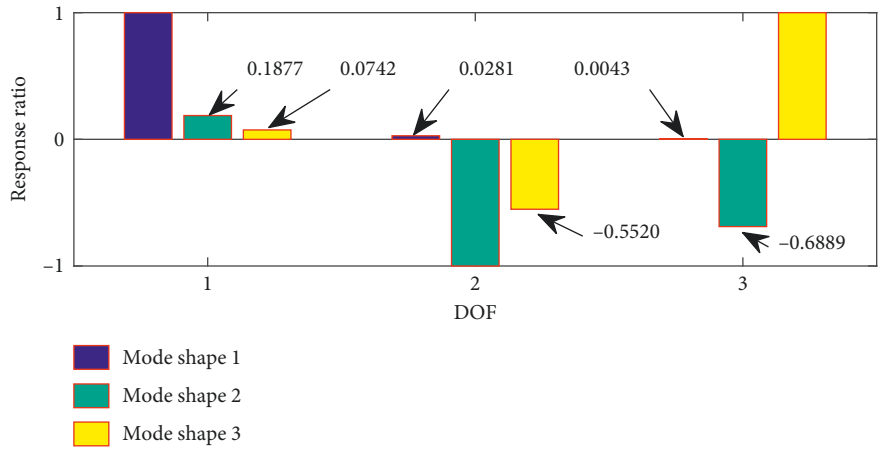

Figure 6: Vibration modes of Model B (Case 3). Mode 1: 1.37 Hz; mode 2: 95.9 Hz; mode 3: 9.72 Hz; dof1: sprung mass; dof2: static mass; dof3: rotating mass.

rotating mass basically remain motionless. It is consistent with that of Model A. At the second shape, the static mass vibration takes predominance. The sprung mass and rotating mass also have some vibration. And the vibration direction of sprung mass is opposite to the wheel, which will increase suspension deformation. The rotating mass vibration prevails at the third shape. Besides that, the static mass and sprung mass also have some degree vibration. The vibration direction of rotating mass is opposite to the static mass, which will increase SRM airgap deformation. And the airgap deformation affects vehicle vibration and vertical force, reversely.

4.2. Amplitude-Frequency Analysis. Amplitude-frequency characteristics describe the transfer response of the IWM-EV system to sinusoidal road excitations, which is the external concrete manifestation of internal characteristics of the system. To obtain the new structure of IWM-EV effect on vehicle performance under stability condition, the amplitude-frequency characteristics of Model and Model B (Case 3) are compared.

The amplitude-frequency sprung mass acceleration, tyre deformation, airgap deformation, and suspension deformation are given important consideration to study vehicle safety and comfort, as shown in Table 8.

In order to study IWM-EV frequency response, Fourier transform is applied to the IWM-EV model. The vehicle dynamic equations (1)–(3), (13), and (14) are transformed as follows:

$$z_1\left(-\omega^2 m_1 + j\omega c_1 + k_1\right) = z_2\left(j\omega c_1 + k_1\right), \quad (24)$$

$$z_2\left(-\omega^2 m_2 + j\omega c_1 + k_1 + k_v\right) = z_1\left(j\omega c_1 + k_1\right) + k_v z_3, \quad (25)$$

$$z_3\left(-\omega^2 m_3 + j\omega c_3 + k_2 + k_v - k_3\right) = z_2\left(k_2 + k_3\right) + q\left(j\omega c_3 - k_3\right). \quad (26)$$

Table 8: Amplitude-frequency response.

Response signal	Description
Vehicle sprung mass acceleration	Vehicle comfort
Tyre deformation	Vehicle safety and stability
Airgap deformation	SRM safety
Suspension deformation	Suspension safety

Denote $A_1 = -\omega^2 m_1 + j\omega c_1 + k_1$, $A_2 = j\omega c_1 + k_1$, $A_3 = -\omega^2 m_2 + j\omega c_1 + k_1 + k_v$, $A_4 = j\omega c_1 + k_1$, $A_5 = -\omega^2 m_3 + j\omega c_3 + k_2 + k_v - k_3$, $A_6 = k_2 + k_3$, $A_7 = j\omega c_3 - k_3$.

According to Equations (24)–(26), vehicle sprung mass vibration response to road excitement is

$$|H(j\omega)|_{\ddot{z}_1 \sim \dot{q}} = \left|\frac{\ddot{z}_1}{\dot{q}}\right| = \omega\left|\frac{z_1}{q}\right| = \omega\left|\frac{A_2 A_7 k_v}{A_1 A_3 A_5 - A_2 A_4 A_5 - A_1 A_6 k_v}\right|. \quad (27)$$

And the wheel bounce, SRM airgap, and suspension deformation response to road excitation are calculated, respectively, as follows:

$$|H(j\omega)|_{z_3 - q \sim \dot{q}} = \left|\frac{z_3 - q}{\dot{q}}\right| = \frac{1}{\omega}\left|\frac{z_3 - q}{q}\right| = \frac{1}{\omega}\left|\frac{A_6}{A_5}\frac{A_1 A_7 k_v}{A_1 A_3 A_5 - A_2 A_4 A_5 - A_1 A_6 k_v} + \frac{A_7}{A_5} - 1\right|, \quad (28)$$

$$|H(j\omega)|_{z_2 - z_3 \sim \dot{q}} = \left|\frac{z_2 - z_3}{\dot{q}}\right| = \frac{1}{\omega}\left|\frac{z_2 - z_3}{q}\right| = \frac{1}{\omega}\left|\frac{A_7 k_v}{A_1 A_3 A_5 - A_2 A_4 A_5 - A_1 A_6 k_v} \cdot \frac{A_2 A_5 - A_1 A_6}{A_5} + \frac{A_7}{A_5}\right|, \quad (29)$$

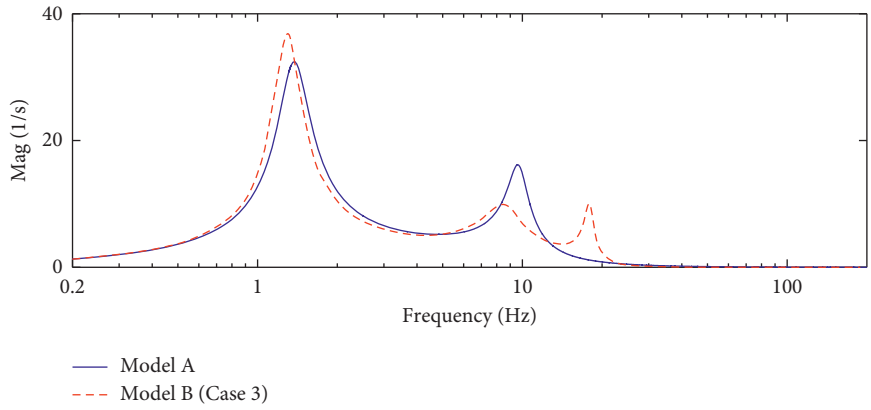

Figure 7: Comparison of sprung mass acceleration response to road excitation.

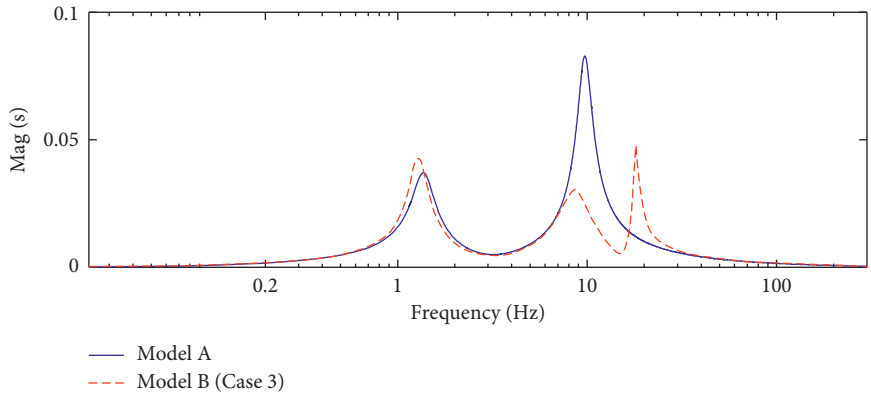

Figure 8: Comparison of wheel bounce response to road excitation.

$$|H(j\omega)|_{z_1-z_2\sim\dot{q}} = \left|\frac{z_1-z_2}{\dot{q}}\right| = \frac{1}{\omega}\left|\frac{z_1-z_2}{q}\right| = \frac{1}{\omega}\left|\frac{(A_2-A_1)A_7k_v}{A_1A_3A_5-A_2A_4A_5-A_1A_6k_v}\right|. \quad (30)$$

According to Equations (27)–(30), the amplitude-frequency responses of Model A and Model B (Case 3) are shown in Figures 7–10. Figure 7 shows that the vehicle sprung mass acceleration of Model B (Case 3) is larger than that of Model A in the vehicle-body resonance region. It means that SRM vertical force has great negative effect on vehicle vibration in the vehicle-body resonance region. In the wheel resonance region, the response of Model B (Case 3) has two peak values at 8.63 Hz and 18.11 Hz, respectively. It is due to the resonance of static mass and rotating mass, as shown in Table 7. The two resonance frequencies enlarge the wheel resonance region, which will take negative effect on wheel bounce.

Figure 8 shows the wheel bounce of Model A and Model B (Case 3). In the vehicle-body resonance region, the peak value of Model B (Case 3) has small increase. On the other hand, the wheel resonance region is enlarged due to the resonance of static mass and rotating mass. However, the peak value of Model B (Case 3) is decreased in the wheel resonance region.

This means that the new structure of IWM-EV will increase vehicle body vibration and enlarge the wheel resonance region, which will affect vehicle safety.

Figure 9 shows SRM airgap deformation of Model B (Case 3). It can be seen that the airgap deformation reaches the peak value in the region of rotating mass resonance. This means the resonance of rotating will form due to large airgap deformation, which will destroy the driven motor. However, the traditional structure does not exist this problem. Figure 10 shows the suspension deformation of Model A and Model B (Case 3). It can be seen that the peak value of suspension deformation has some increase in Model B (Case 3). It means that the new structure will increase suspension deformation, which is easy to destroy suspension block.

5. Conclusions

Based on the proposed vehicle system dynamics model, the new structure effect on IWM-EV stability performance is studied in this paper.

The new structure of IWM-EV has a negative effect on vehicle stability performance. The SRM vertical force will change vehicle stability characteristics. In some severe cases, it will even destroy IWM-EV stability. If the

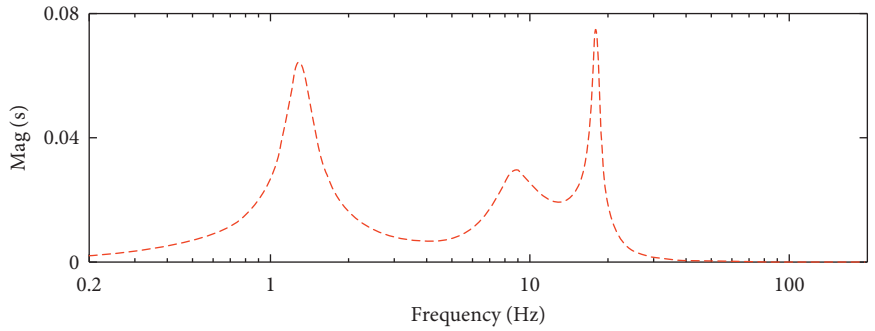

Figure 9: Comparison of SRM airgap deformation response to road excitation.

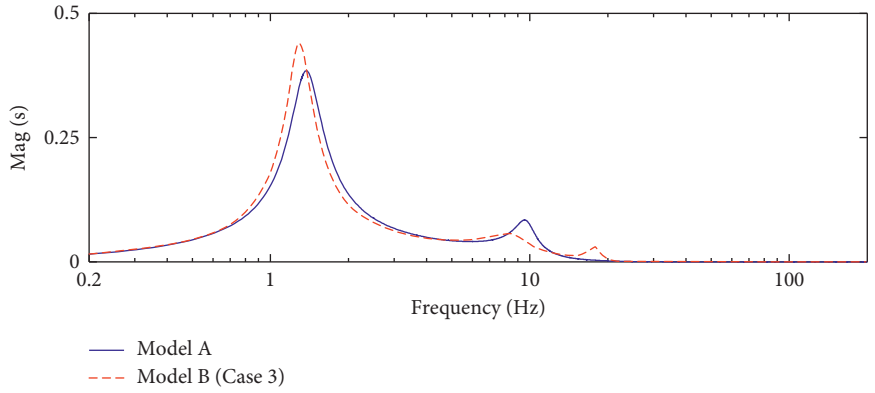

Figure 10: Comparison of suspension deformation response to road excitation.

equivalent coefficient k_v of SRM vertical force belongs to the range of $(-8 \times 10^6$ N/m, 6.25×10^8 N/m], the vehicle is the stability system. Otherwise, the stability of the vehicle system is lost. Without stability, vehicle safety, comfort, maneuverability, and other performance are not possible.

The new structure of IWM-EV has negative effect on vehicle performance under stability condition. The third natural frequency was introduced by the SRM vertical force and airgap deformation. It will cause a new resonance region, which will further effect vehicle vibration. And SRM vertical force and airgap deformation will be affected reversely. It is easy to cause the resonance of the vehicle body, rotating mass, and static mass. In detail, SRM airgap deformation has negative effect on vehicle body vibration, which will decrease vehicle comfort. SRM vertical force has negative effect on the wheel, which will enlarge the vehicle-wheel resonance region. Besides that, SRM vertical force also has some negative effect on SRM airgap deformation, which will reduce SRM safety and stability in operation. Such negative effects cannot be ignored in IWM-EV practical control and design.

There are also some further studies that can be conducted. For example, the effect of the longitudinal force component of SRM vertical force on vehicle dynamics is not considered here, which is another key factor to IWM-EV dynamics, especially to the longitudinal dynamics of vehicle and tyre vibration. Also, finite element analysis and relative experiments are not taken into account in this paper, which is a more complicated issue and needs further investigation.

Data Availability

The datasets used to support this study are currently under embargo while the research findings are commercialized. Requests for data, 12 months after initial publication, will be considered by the corresponding author.

Conflicts of Interest

The authors declare that they have no conflicts of interest.

Acknowledgments

This research was supported by the National Natural Science Foundation of China (Grant no. 51605390), Foundation of Educational Commission of Sichuan Province (Grant no. 16ZA0161), The Open Research Subject of Key Laboratory of Sichuan Provincial Automotive Engineering (Grant no. szjj2015-048), and Foundation of the Science and Technology Research and Development Program of Sichuan Province (Grant no. 2017GZ0103).

References

[1] J.-S. Hu, Y. Wang, H. Fujimoto, and Y. Hori, "Robust yaw stability control for in-wheel motor electric vehicles," *IEEE/*

ASME Transactions on Mechatronics, vol. 22, no. 3, pp. 1360–1370, 2017.

[2] L. Zhai, R. Hou, T. Sun, and S. Kavuma, "Continuous steering stability control based on an energy-saving torque distribution algorithm for a four in-wheel-motor independent-drive electric vehicle," *Energies*, vol. 11, no. 2, p. 350, 2018.

[3] Y.-Y. Wang and F.-N. Yang, "The new structure effect on in-wheel motored vehicle performance," in *Proceedings of 2017 2nd IEEE International Conference on Intelligent Transportation Engineering (ICITE)*, pp. 42–47, Singapore, September 2017.

[4] M. Liu, F. Gu, and Y. Zhang, "Ride comfort optimization of in-wheel-motor electric vehicles with in-wheel vibration absorbers," *Energies*, vol. 10, no. 10, p. 1647, 2017.

[5] T. Kobayashi, E. Katsuyama, H. Sugiura, E. Ono, and M. Yamamoto, "Direct yaw moment control and power consumption of in-wheel motor vehicle in steady-state turning," *Vehicle System Dynamics*, vol. 55, no. 1, pp. 104–120, 2017.

[6] B. Peng, H. Zhang, F. Xuan, and W. Xiao, "Torque distribution strategy of electric vehicle with in-wheel motors based on the identification of driving intention," *Automotive Innovation*, vol. 1, no. 2, pp. 140–146, 2018.

[7] M. S. Kumar and S. T. Revankar, "Development scheme and key technology of an electric vehicle: an overview," *Renewable and Sustainable Energy Reviews*, vol. 70, pp. 1266–1285, 2017.

[8] N. R. Patel, V. A. Shah, and M. Lokhande, "A novel approach to the design and development of 12/15 radial field C-core switched reluctance motor for implementation in electric vehicle application," *IEEE Transactions on Vehicular Technology*, vol. 67, no. 9, pp. 8031–8040, 2018.

[9] M. Takiguchi, H. Sugimoto, N. Kurihara, and A. Chiba, "Acoustic noise and vibration reduction of SRM by elimination of third harmonic component in sum of radial forces," *IEEE Transactions on Energy Conversion*, vol. 30, no. 3, pp. 883–891, 2015.

[10] M. Divandari and A. Dadpour, "Radial force and torque ripple optimization for acoustic noise reduction of SRM drives via fuzzy logic control," in *Proceedings of Industry Applications (INDUSCON), 2010 9th IEEE/IAS International Conference*, pp. 1–6, São Paulo, Brazil, November 2010.

[11] I. Husain, A. Radun, and J. Nairus, "Unbalanced force calculation in switched-reluctance machines," *IEEE Transactions on Magnetics*, vol. 36, no. 1, pp. 330–338, 2000.

[12] Y. A. Beromi, Z. Moravej, and S. Darabi, "Torque ripple reduction of switched reluctance motor using PID fuzzy logic controller," in *Proceedings of International Conference and Exposition on Electrical and Power Engineering*, pp. 456–459, Iaşi, Romania, October 2012.

[13] J. Li and Y. Cho, "Dynamic reduction of unbalanced magnetic force and vibration in switched reluctance motor by the parallel paths in windings," *Mathematics and Computers in Simulation*, vol. 81, no. 2, pp. 407–419, 2010.

[14] H. Inagaki, H. Kato, H. Kuzuya, M. Sugiyama, K. Ikeda, and N. Sebe, "Drive train vibration and acoustic noise reduction control of switched reluctance motor for electric vehicle," in *Proceedings of SAE Technical Papers*, Agra, India, December 2002.

[15] J. Furqani, M. Kawa, and K. Kiyota, "Approximation of radial force in highly saturated region of switched reluctance motor C," in *Proceedings of 2016 19th International Conference on Electrical Machines and Systems (ICEMS)*, IEEE, Chiba-shi, Japan, November 2016.

[16] Y. Wang, Y. Li, W. Sun, and L. Zheng, "Effect of the unbalanced vertical force of a switched reluctance motor on the stability and the comfort of an in-wheel motor electric vehicle," *Proceedings of the Institution of Mechanical Engineers, Part D: Journal of Automobile Engineering*, vol. 229, no. 12, pp. 1569–1584, 2015.

[17] W. Sun, Y. Li, J. Huang, and N. Zhang, "Vibration effect and control of in-wheel switched reluctance motor for electric vehicle," *Journal of Sound and Vibration*, vol. 338, pp. 105–120, 2015.

[18] Y. Wang, P. Li, and G. Ren, "Electric vehicles with in-wheel switched reluctance motors: Coupling effects between road excitation and the unbalanced radial force," *Journal of Sound and Vibration*, vol. 372, pp. 69–81, 2016.

[19] L. Jiongkang, K. W. E. Cheng, Z. Zhu, and X. Xiangdang, "Experimental investigation of in-wheel switched reluctance motor driving system for future electric vehicles," in *Proceedings of PESA 2009. 3rd International Conference on Power Electronics Systems and Applications*, pp. 1–6, Hong-Kong, May 2009.

[20] A. Labak and N. C. Kar, "Outer rotor switched reluctance motor design for in-wheel drive of electric bus applications," in *Proceedings of International Conference on Electrical Machines*, pp. 418–423, Marseille, France, September 2012.

[21] R. Krishnan, *Switched Reluctance Motor Drives–Modeling, Simulation, Analysis, Design, and Applications*, CRC Press, Boca Raton, FL, USA, 2001.

[22] S. Abbasbandy and T. A. Viranloo, "Numerical solution of fuzzy differential equation by Runge-Kutta method," *Journal of Science Teacher Training University*, vol. 1, 2001.

[23] J. Villadsen and M. L. Michelsen, *Solution of Differential Equation Models by Polynomial Approximation*, Prentice-Hall, Englewood Cliffs, NJ, USA, 1978.

[24] S. Ayari, M. Besbes, M. Lecrivain, and M. Gabsi, "Effects of the airgap eccentricity on the SRM vibrations," in *Proceedings of IEEE International Electric Machines and Drives Conference IEMDC'99*, pp. 138–140, IEEE, Seattle, WA, USA, May 1999.

[25] N. R. Garrigan, W. L. Soong, C. M. Stephens, A. Storace, and T. A. Lipo, "Radial force characteristics of a switched reluctance machine," in *Proceedings of Industry Applications Conference, 1999. Thirty-Forth IAS Annual Meeting*, IEEE, Maryland, MD, USA, October 1999.

[26] E. Casetti and J. P. Jones III., *Applications of the Expansion Method*, Routledge, London, UK, 2003.

[27] S. Sadeghi, "Dynamic modeling and simulation of a switched reluctance motor in electric vehicles," *Acta Polytechnica Hungarica*, vol. 7, pp. 51–71, 2010.

[28] R. C. Dorf and R. H. Bishop, *Modern Control Systems*, Pearson, Turin, Italy, 2011.

[29] Y. J. Kim and J. S. Bolton, "Effects of rotation on the dynamics of a circular cylindrical shell with application to tire vibration," *Journal of Sound and Vibration*, vol. 275, no. 3, pp. 605–621, 2004.